Fused Deposition Modeling of Polymethylmethacrylate for Use in Patient-Specific Reconstructive Surgery

David Espalin[a], Karina Arcaute[a], David Rodriguez[a], Frank Medina[a], Matthew Posner[b], Ryan Wicker[a]

[a] *The University of Texas at El Paso, W.M. Keck Center for 3D Innovation, College of Engineering, El Paso, TX 79968-0521*
[b]*William Beaumont Army Medical Center*

Abstract

Polymethylmethacrylate (PMMA) is a biocompatible alloplastic material used in craniofacial reconstruction and as bone cement and antibiotic-impregnated spacers in orthopaedics. The polymerization of PMMA in-situ causes tissue necrosis and other complications due to the long surgical times associated with mixing and shaping the PMMA. PMMA is a thermoplastic acrylic resin suitable for extrusion in FDM thus 3D anatomical models can be fabricated prior to surgery directly from medical imaging data. The building parameters required for successful FDM fabrication with medical-grade PMMA filament (1/16"Ø) were developed using an FDM 3000. It was found that a liquefier and envelope temperature of 235ºC and 55ºC, respectively, as well as increasing the model feed rate by 60%, were necessary to properly and consistently extrude the PMMA filament. Scaffolds with different porosities and fabrication conditions (tip wipe frequency and layer orientation) were produced, and their compressive mechanical properties were examined. Results show that both the tip wipe frequency (1 wipe every layer or 1 wipe every 10 layers) and layer orientation (transverse or axial with respect to the applied compressive load) used to fabricate the scaffolds, as well as the porosity of the scaffold had an effect on the mechanical properties. The samples fabricated with the high tip frequency had a larger compressive strength and modulus (Compressive strength: 16 ± 0.97 vs. 13 ± 0.71 MPa, Modulus: 370 ± 14 vs. 313 ± 29 MPa, for samples fabricated in the transverse orientation with 1 tip wipe per layer or 1 tip wipe per 10 layers, respectively). Also, the samples fabricated in the transverse orientation had a larger compressive strength and modulus than the ones fabricated in the axial orientation (Compressive strength: 16±0.97 vs. 13±0.83 MPa, Modulus: 370±14 vs. 281±22 MPa, for samples fabricated with 1 tip wipe per layer, in the transverse and axial orientation, respectively). Overall, the compressive strain for the samples fabricated with the four different conditions ranged from 8 – 12%. In regards to the porosity of the samples, in general, the stiffness, yield strength and yield strain decreased when the porosity increased (Compressive strength: 12±0.71 – 7±0.95 MPa, Modulus: 248±10 – 165±16 MPa, Strain: 7±1.5 – 5±1% for samples with a porosity ranging from 55 – 70%). The successful FDM fabrication of patient-specific, 3D PMMA implants with varying densities, including the model of a structure to repair a cranial defect and the model of a femur, was demonstrated. This work shows that customized structures with varying porosities to achieve tailored properties can be designed and directly fabricated using FDM and PMMA.

1. Introduction

Fabricating reconstructive structures has been accomplished with many techniques and technologies including traditional methods such as solvent casting, fiber-bonding, membrane lamination, melt molding, and gas forming. While these methods have been adopted in the medical industry, they do not provide structures with consistent interconnected pore networks and uniform microstructures [Zein *et al*., 2002]. Reconstructive structures are developed and fabricated to play very specific roles including temporary bone spacers, antibiotic delivery devices, permanent bone substitutes, biodegradable bone structures, etc. Reconstructive structures are necessary in correcting bone injuries due to trauma, bone tissue loss after tumor surgery, and congenital bone malformations, or in providing a temporary spacer in the case of bone implant failure due to infection [Eufinger *et al*. 1995; Materialise, 2009; Lee *et al*., 2009; Frutos Cabanillas *et al*., 2000, Pelletier *et al.*, 2009].

Polymethylmethacrylate (PMMA) is an FDA approved synthetic biomaterial widely used to fabricate reconstructive structures, including dental implants, reconstruction of craniofacial defects, or as bone cement to remodel lost bone and affix implants. Commercially available PMMA bone cements include powder constituents of prepolymerized PMMA, an initiator that catalyzes the polymerization process and a radiopacifier. Liquid constituents contain large amounts of monomer (MMA), an accelerator that breaks down the catalyst, and a stabilizer that impedes premature polymerization [Lewis, 1997].

PMMA is commonly used in orthopedic surgery in the form of the two-component system described previously. Mixing of both components is conducted and inserted into the surgery site where polymerization occurs. There are several main drawbacks with the technique. Polymerization of PMMA in-situ causes tissue necrosis, weakened local blood circulation and tendency to membrane formation all of which are associated with the high exothermic temperature, ranging from 67°C to 124°C, of the bone cement. Also, bone necrosis is caused by unreacted MMA monomer before complete polymerization. Another complication is the size reduction of the bone cement during the polymerization process. There is also a significant stiffness difference between PMMA and the contiguous bone and risk of infection due to the large operating times [Lewis, 1997; Eufinger *et al*. 1995].

In order to avoid the drawbacks of polymerizing PMMA in-situ, other processing methods for PMMA have been attempted, including casting and compression molding in a cavity mold created from the master implant made in an additive manufacturing (AM) or rapid prototyping (RP) technology from medical imaging data prior to implantation surgery [Gopakumar, 2004; Lee *et al*., 2009, Materialise, 2009]. The molded PMMA implant can be sterilized by gas or radiation sterilization or by autoclaving. Some other researchers have used RP models of the bone defect to model the implant prior or in the surgery site [Lee *et al*., 2009, Materialise, 2009].

PMMA is a suitable material to use in fused deposition modeling (FDM). Fused deposition modeling is an additive manufacturing (AM) technology that allows fabrication of complex three-dimensional geometries layer-by-layer. A filament of thermoplastic material is driven at a controlled rate into a liquefier that is heated to a prescribed temperature associated

with the material being used. The material is extruded in a semi-molten state through a small diameter nozzle while the head scans a building stage along a programmed toolpath. Upon completion of the layer, the stage lowers a predefined Z distance and successive layers are created in the same fashion. PMMA has a melting temperature range (200°C to 230°C) [Osswald *et al*., 2006] that lies within FDM operating temperatures (up to 290°C). Another advantage is that PMMA has a low water absorption capability (0.35%), which inhibits moisture collection that can cause problems in the FDM extrusion process. The characteristics of parts fabricated in FDM are influenced by material properties and processing parameters that include extrusion/envelope temperature, material feed rate, slice height (SH), road width (RW), raster angle (RA), deposition layer orientation, air gap (AG) and contour styles.

This study initiates an effort at processing PMMA via FDM for medical applications including the creation of non-load bearing reconstructive bone structures and temporary bone spacers in an attempt to improve the current state of the use of PMMA in these applications. The effect of different fabrication conditions on mechanical properties and porosity of PMMA parts fabricated in FDM, as well as the relation between mechanical properties and porosity of PMMA parts were examined.

2. Materials and methods

2.1. FDM system optimization

Adapting the FDM 3000 system (Stratasys Inc., Eden Prairie, MN) to properly and consistently extrude PMMA filament (Biogeneral Inc., San Diego, CA) required identifying parameters that dictate extrusion regardless of material and determining the suitable parameter values for PMMA. Extrusion with FDM primarily depends on liquefier temperature, envelope temperature and material feed rate. Simple square prisms were fabricated with T16 tips, an envelope temperature of 75°C and various liquefier temperatures while closely monitoring the building process. Relatively low temperatures, 180°C - 210°C, failed to properly extrude PMMA as the filament would audibly break before entering the liquefiers. A temperature of 225°C allowed PMMA extrusion but created extremely stiff rasters that would not properly adhere to the support material (ABS P400 R) resulting in models detaching before proper completion. Higher temperatures of about 270°C created rasters with visible wavy surfaces and left material residue that affected geometry. Additionally, excessive material flowed from the extruding tips while the FDM system was not building. A liquefier temperature of 235°C was found to have the best raster surfaces and the minimum evidence of material residue for this envelope temperature. Various envelope temperatures were tested and it was found that 55°C was optimal in minimizing material residue and enhancing raster surfaces. Material feed rates were determined by executing the default calibration method supplied by the Insight V3.5 slicing software (Stratasys Inc., Eden Prairie, MN) until proper raster widths were achieved.

2.2. Experimental design

Two experimental designs were carried out to determine the effect of different factors (fabrication conditions and scaffold characteristics) on the mechanical properties of the fabricated structures as described in Table 1. Experimental Design I analyzed the effect of tip

Table 1. Design of experiments

	Conditions	Sample Criteria
Experiment I	tip wipe frequency	1 tip wipe/layer 1 tip wipe/10 layers
	anisotropy	transverse axial
Experiment II	porosity	55% 63% 66% 70%

wipe frequency and anisotropy on the mechanical properties of the fabricated structures, while Experimental Design II evaluated the mechanical properties of samples with different porosity percentages. Each experimental condition consisted of 6 square prism specimens with design dimensions 7 x 7 x 13.5 mm. The scaffold structures were designed by maintaining a 0.406mm RW, 0.254mm SH and 0°/90° RA. AG was varied in order to achieve different porosity ranges. Slicing and toolpath parameters are illustrated in Figure 1.

2.2.1. Tip wipe frequency

FDM systems constantly clean the extruding tips by wiping them against a brass brush or a rubber. When a part is manufactured, the parameters for tip wipe configuration can be set at different values to produce cleaner parts or to save time and material. In the default configuration the system does a tip wipe after depositing ten layers (1wipe per 10 layers). A tip wipe every deposited layer (1 wipe per layer) is usually configured in order to produce cleaner parts with less contamination or blend of materials between layers. For Experimental Design I, two different tip wipe frequencies were tested: 1 wipe every ten layers, and 1 wipe every layer.

2.2.2. Layer orientation

Two different layer orientations were tested for Experimental Design I, with one having layer orientations in the transverse position relative to applied force and the other orientated in the axial position as illustrated in Figure 2. These two layer orientations were selected to determine anisotropic influences on mechanical properties of the samples.

2.2.3. Percent porosity

A range of porosities within the 50-70% range was achieved by varying the AG in the scaffold design. The effect of the scaffold percent porosity on the mechanical properties of the structures was evaluated in Experimental Design II.

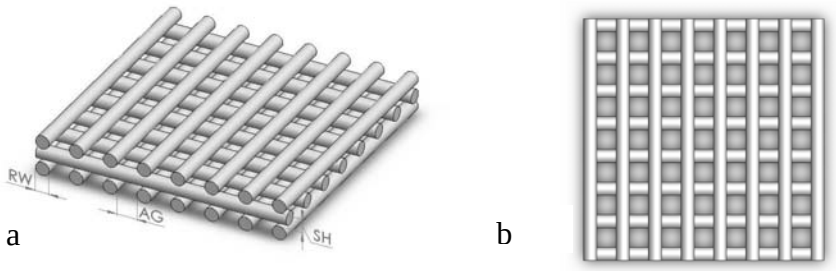

Figure 1. Slicing and toolpath parameters (a) trimetric view illustrating road width (RW), air gap (AG) and slice height (SH), (b) top view with 0°/90° RA.

2.3. Scaffold characterization

The fabricated scaffolds were characterized in terms of their mechanical properties and porosity. The samples were tested in compression to evaluate their yield strength, yield strain and modulus of elasticity. The samples were weighted and their dimensions were evaluated to estimate the porosity. Furthermore, the specimens for Experimental Design II were imaged in order to measure the RW, AG and SH of the fabricated scaffold, and compare the measured values versus the design values.

2.3.1. Porosity

Porosity estimates were achieved by correlating scaffold geometrical dimensions and material density as per ASTM F 2450-04. The scaffold volume, V_T, was determined from caliper measurements of length, width, and height. Utilizing the material density of 1.17g/cm^3 [Osswald *et al.*, 2006] the following equation was employed:

$$V_p = V_T - \frac{m_s}{\rho_s}$$

where V_P is the total volume occupied by the network of pores, m_s is the total specimen mass determined using a Sartorius CP124S micro-balance (Sartorius Stedium SUS Inc., Concord, CA) and ρ_s is the material density. Percentage of porosity was calculated according to:

$$Porosity = \frac{V_P}{V_T} \times 100$$

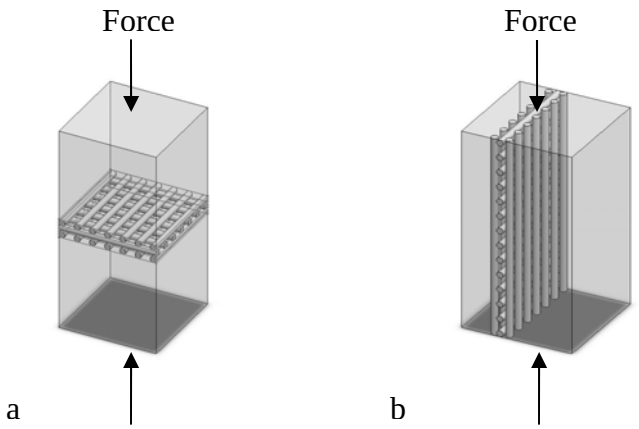

Figure 2. Layer orientations relative to compressive load (a) transverse (b) axial.

2.3.2. Compressive testing

Compressive tests were conducted following guidelines provided by ASTM F 451-08 on an Instron 5866 system (Instron®, Norwood, MA). A 10 kN load cell was used and a deformation cross head speed of 1 mm/min was employed. Compressive stress calculations were carried out by dividing the applied force by the original specimen cross-sectional area. Strain was defined as the ratio of axial deformation to original specimen height. Compressive stress-strain graphs were created from which several mechanical properties were acquired. Compressive yield strength was defined as the stress after which the initial linear region deviated from linearity; yield strain is the strain associated with the compressive yield strength. The stiffness is defined as the modulus of elasticity, E, and was calculated from data representing the slope of the initial linear region.

2.3.3. Imaging

Specimens for Experimental Design II were observed and imaged using a stereomicroscope (Leica MZ16, Leica Microsystems Inc., Bannockburn, IL) equipped with a CCD camera (Retiga 2000R Fast 1394, QImaging Corp., Canada). Measurements for the RW, AG and SH were taken from digital images. Several images were captured in order to take at least five measurements per dimension per sample.

2.4. Statistical analysis

For all experiments, student's t-tests were performed to compare mean values of independent samples with a significance level of 0.05. In addition, an ANOVA test was performed for the specimens used in Experimental Design II to compare RW mean values of six independent samples with a significance level of 0.05. Data in graphs represents averages ± one standard deviation.

3. Results and discussion

3.1. Experimental design I

The results on mechanical properties and porosity for samples built with different tip wipe frequencies and layer orientations are summarized graphically in Figure 3. Also, Table 2 contains physical data (mass, volume, and estimated porosity) for the samples. It is important to note that contraction and inner stresses develop in the recently deposited layer as it cools from the extruded temperature to the envelope temperature [Wang *et al.*, 2007]. If the envelope temperature lies within the extruded and material glass-transition temperature range, stress will not accumulate amongst layers, therefore inhibiting the structure from withstanding higher stresses. The research presented here allowed the envelope temperature to be lower than the PMMA glass-transition temperature of 130°C to promote higher stress resistance. When utilizing one tip wipe per layer, this increases the time between layer deposition causing differences in scaffold characteristics discussed below.

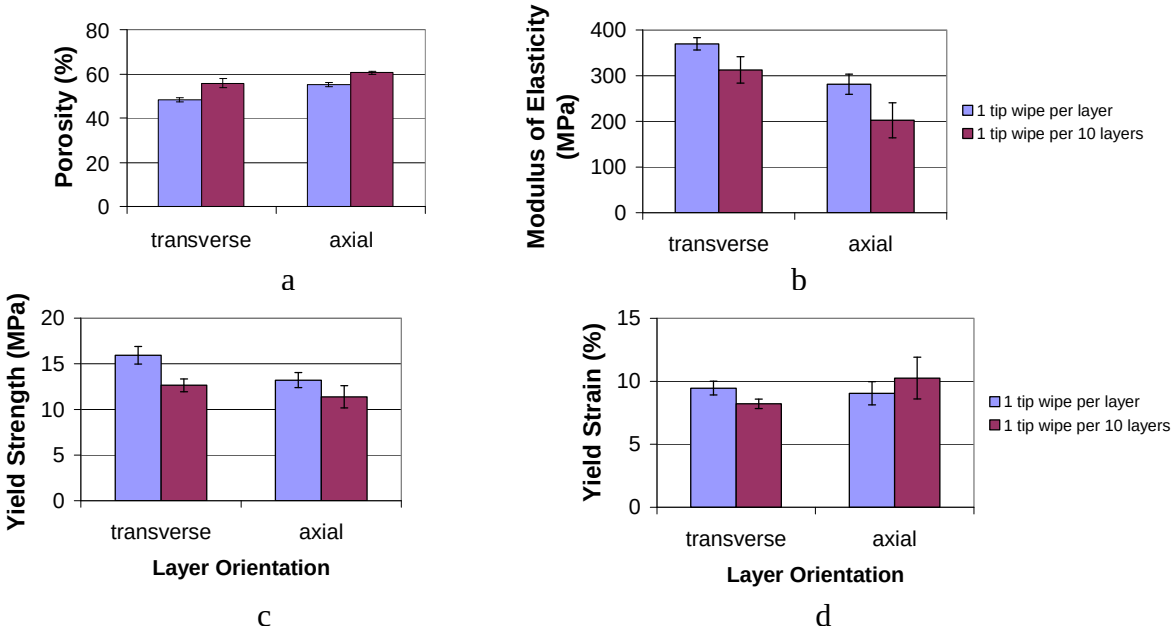

Figure 3. Experiment I compressive test results (a) percent porosity, (b) stiffness, (c) yield strength, (d) yield strain.

3.1.1. Porosity

Porosities and physical properties are reported in Table 2. In general, V_T, V_P, and porosity were higher when fabricating with one tip wipe per 10 layers in both the transverse and axial orientations. In the transverse orientation, porosity increased from 48% to 56% when the frequency of tip wipes was reduced from once per layer to once per 10 layers. In the axial orientation, porosity also increased from 55% to 60 % when tip wipes were used less frequently. Student's t-test results indicated that the effect of tip wipes was statistically significant as $p \leq 0.05$ for both transverse and axial orientations. Samples fabricated with one tip wipe per 10

layers had less elapsed time between layer deposition that resulted in minimized contraction and promoted larger V_T, V_P and percent porosity.

Primary differences in mass originated from more model volume required for the transverse position that inherently decreasing porosity due to layer orientation (student's t-test, $p \leq 0.05$). Additionally, each layer required a tool start and stop operation which resulted in residue material that unintentionally increased the scaffold mass. Since the transverse layer position required 54 layers compared to 28 axial layers, more residue material was collected that simultaneously increased the mass and decreased the porosity as illustrated in Figure 3a. Therefore, the axial layer position achieved 55% porosity and the transverse position resulted in 48% porosity.

Table 2. Experiment I porosities and physical properties.

	Transverse		Axial	
	1 tip wipe per layer	1 tip wipe per 10 layers	1 tip wipe per layer	1 tip wipe per 10 layers
Average mass (g)	0.3813	0.378	0.3271	0.3282
Average V_T (mm^3)	0.630	0.732	0.623	0.709
Average V_P (mm^3)	0.304	0.409	0.344	0.429
Average Porosity (%)	48	56	55	60

3.1.2. Compressive yield strength

Results reported in Figure 3c found that yield strength decreased from 16 MPa to 13 MPa when decreasing the frequency of tip wipes in the transverse orientation. Similarly, yield strength decreased from 13 MPa to 11 MPa in the axial orientation when tip wipe frequency was decreased. Allowing the recently deposited layers to cool longer when using one tip wipe per layer increased the inner stresses and promoted higher yield strength. In general, yield strength decreased when tip wipe frequency was decreased from once per layer to once every 10 layers (student's t-test, $p \geq 0.05$). Layers positioned in the axial direction provided columns of PMMA in every other layer to support the applied force during compressive testing. In this particular position, 14 layers supported the force whereas the transverse position provided 54 layers to resist the compressive load. Figure 3c illustrates that yield strength was higher (student's t-test, $p \leq 0.05$) in the transverse orientation than in the axial orientation.

3.1.3. Compressive yield strain

Yield strain shown in Figure 3d experienced a decrease from 9% to 8% when the tip frequency was reduced from 1 tip wipe per layer to 1 tip wipe per 10 layers in the transverse orientation. Student's t-test supported the significance, $p \leq 0.05$. The opposite was graphically noted for the axial orientation as yield strain seemingly increased from 9% to 10% when tip wipe frequency was decreased. However, student's t-test results indicated that the effect of tip wipe configuration for the axial orientation was not significant, $p \geq 0.05$.

Transverse and axial orientations experienced a yield strain of ~9% and there is evidence that the means are not different (t-test, $p \geq 0.05$). This indicates that compressive tests yielded identical strains for both layer orientations but a higher yield stress was supported by the transverse layer orientation.

3.1.4. Stiffness

Stiffness was observed to be higher when tip wipes were executed after each layer. In the transverse orientation, stiffness decreased from 370 MPa to 313 MPa when tip wipe frequency was decreased from once per layer to once every 10 layers. In similar fashion, stiffness decreased from 281 MPa to 202 MPa when tip wipe frequency was decreased in the axial orientation. This indicates that the cooling and contraction effect caused by frequent tip wipes allowed and created higher stiffness desirable for bone reconstructive structures (student's t-test, $p \geq 0.05$). Caution must be taken as larger structures may experience significant contraction and complications may arise, therefore yielding non-conforming scaffold dimensions.

Recalling the yield strength and strain results mentioned above, it is expected to find higher stiffness for specimens fabricated in the transverse position. Results supported this hypothesis as stiffness for specimens in the transverse position was calculated to be 370 MPa (axial orientation yielded 281 MPa) with the effect of layer orientation being statistically significant (student's t-test, $p \geq 0.05$).

3.2. Experimental design II

Porosity and compressive testing results are illustrated in Figure 4. Table 3 shows the measured dimensions for RW. SH and AG for the samples. After analyzing the 0.610 mm and 0.800 mm AG samples, it was concluded that there was no significant difference in porosity.

3.2.1. Dimensional characteristics

Stereomicroscope images were analyzed to determine RW, AG and SH. An ANOVA analysis was done on all samples and it was determined that road width means did not differ ($p \geq 0.05$) when values of AG where increased. Actual road width for all samples in Experiment II was determined to be 0.352 ±0.039. The expected 0.406 mm RW was not achieved but the difference was minimal. This difference in RW also caused a slight difference in AG with the largest difference occurring when the actual AG was measured as 2.645 mm and the expected AG was 2.800 mm.

Table 3. Experiment II dimensional characteristics obtained with stereomicroscope.

	Road Width (mm)		Slice Height (mm)		Air Gap (mm)	
	Actual	Expected	Actual	Expected	Actual	Expected
55% Porosity	0.355	0.406	0.243	0.254	0.859	0.800
63% Porosity	0.352	0.406	0.259	0.254	1.255	1.200
66% Porosity	0.328	0.406	0.267	0.254	1.731	1.700
70% Porosity	0.362	0.406	0.467	0.254	2.645	2.800

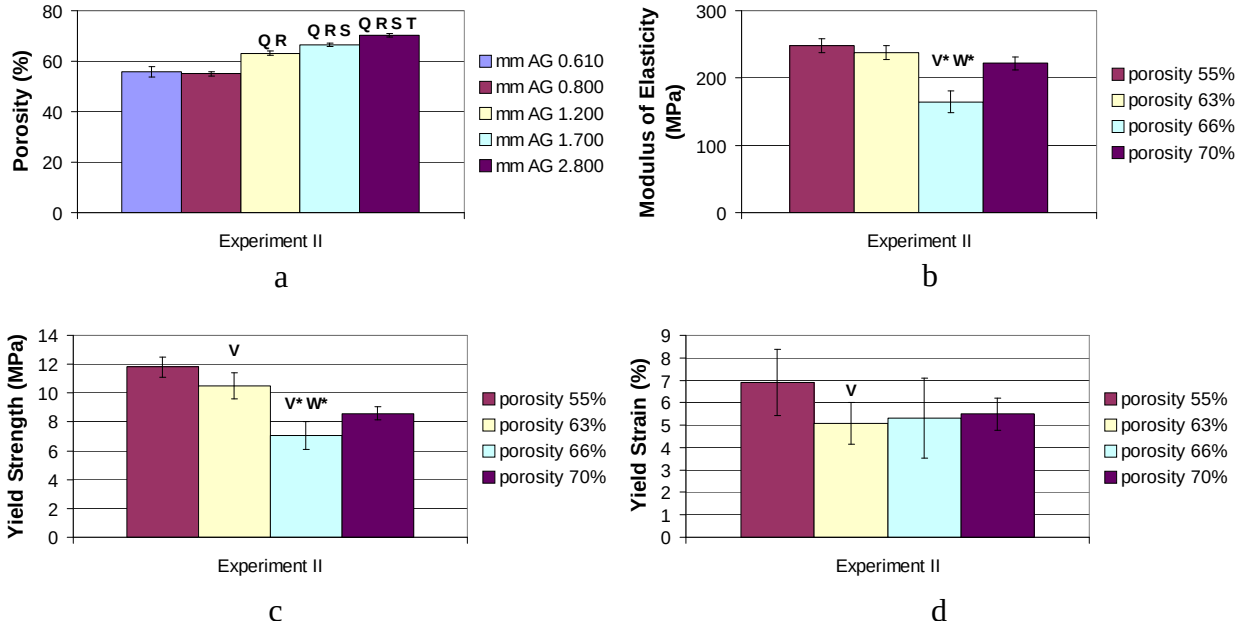

Figure 4. Experiment II: porosity and compressive testing results ($p<0.05$ when compared to "Q" 0.610 mm AG sample, "R" 0.800 mm AG sample, "S" 1.200 mm AG sample, "T" 1.700 mm AG sample, "V" 55% porosity sample, "W" 63% porosity sample, * indicates $p<<0.05$) (a) percent porosity, (b) stiffness, (c) yield strength, (d) yield strain.

Slice heights remained relatively constant when varying AG except in the case of the 70% porosity sample. Careful observations during fabrication revealed that the expected 2.800 mm AG provided insufficient layer-to-layer foundations for deposition, therefore causing the suspended rasters to have a larger slice height. In addition, portion of the layers often collapsed to preceding layers affecting the mechanical properties.

3.2.2. Porosity

As illustrated in Figure 4a, porosity increased as AG was increased resulting in samples of the following percent porosities: 56%, 55%, 63%, 66%, and 70%. This increase is due to V_T remaining relatively constant as m_s decreased and V_P increased when AG increased. Another approach is to associate porosity with the number of rasters required to construct each layer. The least porous specimen is associated with the most number of required rasters, 7 per layer, while the most porous specimen contained 3 rasters per layer. All other specimens follow the same trend as shown in Figure 5.

3.2.3. Compressive yield strength

Major load support was provided at raster overlapping locations that are parallel throughout the entire specimen height as illustrated by shaded areas in Figure 5. Additional

support was provided by the intersecting rasters. A general trend of decreasing yield strength was observed when porosity was increased as illustrated in Figure 4c. This trend held true at all porosities except at the highest porosity achieved, 70%. Layer segments that collapsed onto preceding layers provided added support that allowed higher stress resistance. The faulty fabrication of this sample caused the yield strength, yield strain and stiffness to deviate from the general trend. Excluding the 70% porosity sample, yield strength decreased from 12 MPa to 7 MPa when porosity increased from 55% to 66%.

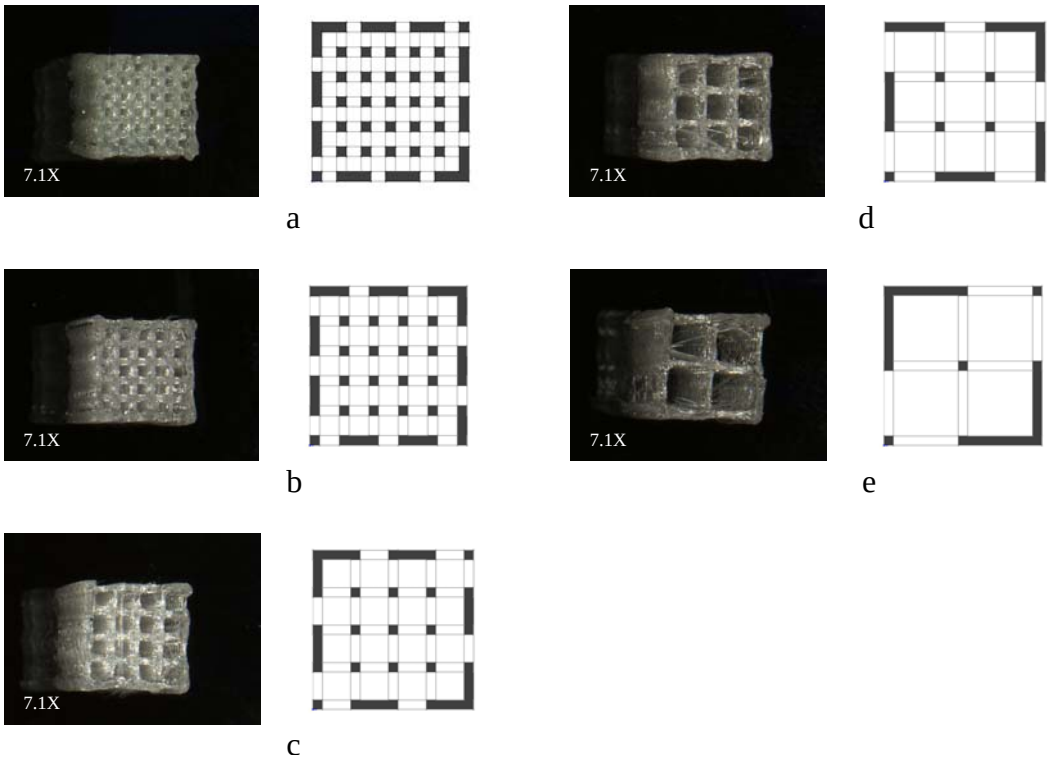

Figure 5. Experiment II: samples of varying porosities with associated overlapping rasters (a) 56% porosity, 0.610 mm AG, 7 rasters per layer, (b) 55% porosity, 0.800 mm AG, 6 rasters per layer, (c) 63% porosity, 1.200 mm AG, 5 rasters per layer, (d) 66% porosity, 1.700 mm AG, 4 rasters per layer, (e) 70% porosity, 2.800 mm AG, 3 rasters per layer. Each sample is accompanied with a representation of overlapping rasters.

3.2.4. Compressive yield strain

Yield strain shown in Figure 4d also followed a decreasing trend when porosity increased with the exception being the 66% and 70% porosity samples. Student's t-test indicated that the 63% and 66% porosity sample means are not different ($p \geq 0.05$). The yield strain anomaly in the 70% porosity sample is also a result of the collapsed layers. Yield strain decreased from 7% to 5% (excluding the 70% porosity sample) when porosity increased from 55% to 66%.

3.2.5. Stiffness

Excluding the 70% porosity sample, stiffness decreased from 248 MPa to 165 MPa when porosity increased from 55% to 66%. This trend is reflective of the trends established by the yield strength and strain. Although the application of this scaffold fabricating process is for non-load bearing structures, higher stiffness is still desirable which was exhibited by the least porous sample.

3.4. Application fabrication of patient-specific 3D models

3D CAD models can be generated from medical imaging data sets acquired through CT scans or MRI by utilizing image processing software such as Mimics® (Materialise NV, Irvine, CA). CAD models can then be tailored to create scaffolds with specific porosities with FDM technology. Figures 6 and 7 show patient-specific, anatomical 3D PMMA models fabricated in a FDM 3000 system, including the model of a cranial defect and the model of a femur. Figure 6a shows an ABS FDM model of a skull with a defect while Figure 6b shows one of the fabricated PMMA models to correct the cranial defect placed in the ABS skull. Figures 6a and 6b show PMMA models with different porosity. Figure 7a shows the PMMA model of a femur during fabrication, and Figure 7b shows the final femur model.

4. Conclusions

The building parameters required for successful FDM fabrication with medical-grade PMMA filament (1/16”Ø) were developed using an FDM 3000. It was found that a liquefier and envelope temperature of 235ºC and 55ºC, respectively, as well as increasing the model feed rate by 60%, were necessary to properly and consistently extrude the PMMA filament. Scaffolds with different porosities and fabrication conditions (tip wipe frequency and layer orientation) were produced, and their compressive mechanical properties were examined. Results show that both the tip wipe frequency (1 wipe every layer or 1 wipe every 10 layers) and layer orientation (transverse or axial with respect to the applied compressive load) used to fabricate the scaffolds, as well as the porosity of the scaffold had an effect on the mechanical properties.

Tip wipe frequency had a direct correlation to contraction and inner stress development. Samples fabricated with 1 tip wipe per layer allowed the development of higher inner stresses that resulted in higher yield strength. Although this may be noted as a benefit, one must be cautious of the geometric changes, specifically shrinkage, which may pose problems for models of larger size. The samples fabricated with the high tip frequency had a larger compressive strength and modulus (Compressive strength: 16 ± 0.97 vs. 13 ± 0.71 MPa, Modulus: 370 ± 14 vs. 313 ± 29 MPa, for samples fabricated in the transverse orientation with 1 tip wipe per layer or 1 tip wipe per 10 layers, respectively).

Specimens fabricated in the transverse orientation yielded desirable mechanical properties due to added support provided by each layer whereas axial orientation specimens only supported loads with every other layer. While porosity did experience a decrease in the transverse orientation compared to the axial orientation, the higher yield strength was seen as a worthwhile benefit. Samples fabricated in the transverse orientation had a larger compressive

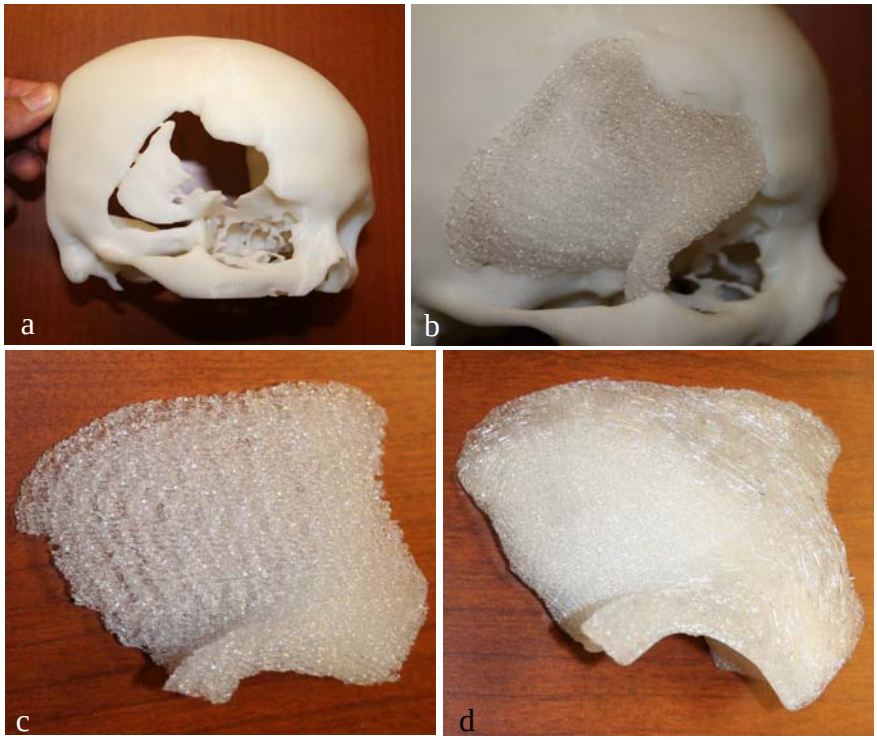

Figure 6. Patient-specific PMMA model to repair a cranial defect. a) ABS model of the skull showing the defect. b) PMMA model to correct the cranial defect placed in the ABS skull. c and d) fabricated PMMA models with different densities.

strength and modulus than the ones fabricated in the axial orientation (Compressive strength: 16±0.97 vs. 13±0.83 MPa, Modulus: 370±14 vs. 281±22 MPa, for samples fabricated with 1 tip wipe per layer, in the transverse and axial orientation, respectively). Overall, the compressive strain for the samples fabricated with the four different conditions ranged from 8 – 12%.

In regards to the porosity of the samples, in general, the stiffness, yield strength and yield strain decreased when the porosity increased (Compressive strength: 12±0.71 – 7±0.95 MPa, Modulus: 248±10 – 165±16 MPa, Strain: 7±1.5 – 5±1% for samples with a porosity ranging from 55 – 70%). The porosity of the samples was increased by increasing the air gap in the scaffold design. It was noticed that extremely large air gaps can cause faulty fabrications of highly porous scaffolds. Alternatives to achieving large porosities include using smaller extrusion tips or smaller road widths.

The successful FDM fabrication of patient-specific, 3D PMMA models with varying densities, including the model of a structure to repair a cranial defect and the model of a femur, was demonstrated. This work showed the possibility of using FDM for the direct fabrication of PMMA customized structures with varying porosities, and therefore tailored mechanical properties.

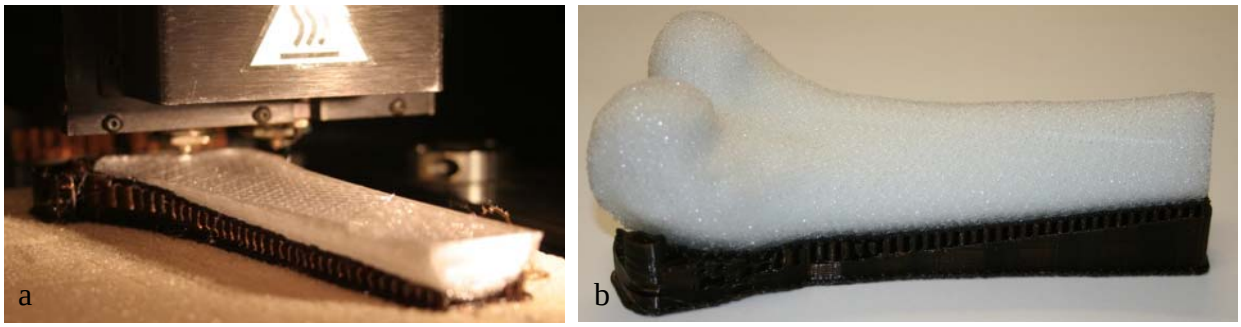

Figure 7. Anatomical PMMA model of a femur: a) during fabrication, the highly porous inside can be observed, b) final fabricated model with support.

Acknowledgments

The research presented here was performed at the University of Texas at El Paso in the W.M. Keck Center for 3D Innovation. Support was provided by the University of Texas System Louis Stokes Alliance for Minority Participation Program under grant NSF-HRD-0703584. The authors are grateful for the assistance of Justin Masias, Eric Anchondo, and Eduardo Basurto of the Keck Center on various aspects of the project. The authors are grateful to Biogeneral, Inc., for participating in the research and providing the PMMA filament used in this study. The authors would also like to thank Stratasys, Inc. for providing the FDM systems used in this study.

References

Cai, Shengyong, and Juntong Xi. 2008. "A control approach for pore size distribution in the bone scaffold based on the hexahedral mesh refinement." *Computer-Aided Design* 40, no. 10/11: 1040-1050.

Eufinger, H., Wehmoller, M., Harders, A., and Heuser, L. 1995. International Journal of Oral and Maxillofacial Surgery. Vol. 24: 104-110.

Gopakumar, S. 2004. "RP in Medicine: A Case Study in Cranial Reconstructive Surgery." *Rapid Prototyping Journal* Vol. 10 No. 3: 207-211.

Frutos Cabanillas, P., Diez Peña, E., Barrales-Rienda, J.M., and Frutos, G. 2000. "Validation and In-vitro Characterization of Antibiotic-loaded Bone Cement Release." *International Journal of Pharmaceutics*: 15-26.

Lee, S.C., Wu, C.T., Lee, S.T., and Chen P.J. 2009. "Cranioplasty Using Polymethyl Methacrylate Prostheses." *Journal of Clinical Neuroscience* 16: 56-63.

Lewis, G. 1997. "Properties of acrylic bone cement: state of the art review." *Journal of Biomedical Materials Research* 38, no. 2: 155-182.

Materialise. 2009. Medical Solutions: Cranioplasty Medical Models. http://www.materialise.com/materialise/view/en/421133-Cranioplasty.html

Osswald, T., Baur, E., Brinkmann, S., Oberbach, K., & Schmachtenberg, E. 2006. *International plastics handbook: the resource for plastics engineers*. Cincinnati: Hanser Gardner Publications.

Pelletier, M.H., Malisano, L., Smitham, P.J., Okamoto, K., and Walsh, W.R. 2009. “The compressive Properties of Bone Cements containing Large Doses of Antibiotics.” *The Journal of Arthoplasty* Vol. 24 No. 3: 454-461.

Tian-Ming Wang, Jun-Tong Xi, and Ye Jin. 2007. "A model research for prototype warp deformation in the FDM process." *International Journal of Advanced Manufacturing Technology* 33, no. 11/12: 1087-1096.

Zein, Iwan, Dietmar W. Hutmacher, Kim Cheng Tan, and Swee Hin Teoh. 2002. "Fused deposition modeling of novel scaffold architectures for tissue engineering applications.” *Biomaterials* 23, no. 4: 1169.